Synergistic Effects and Ecological Responses of Combined In Situ Passivation and Macrophytes toward the Water Quality of a Macrophytes-Dominated Eutrophic Lake

Wei Yu [1,2], **Haiquan Yang** [1,*], **Yongqiong Yang** [2,*], **Jingan Chen** [1], **Peng Liao** [1], **Jingfu Wang** [1], **Jiaxi Wu** [1,3], **Yun He** [1,4] **and Dan Xu** [1]

[1] State Key Laboratory of Environmental Geochemistry, Institute of Geochemistry, Chinese Academy of Sciences, Guiyang 550081, China; yuwei@mail.gyig.ac.cn (W.Y.); chenjingan@vip.skleg.cn (J.C.); liaopeng@mail.gyig.ac.cn (P.L.); wangjingfu@vip.skleg.cn (J.W.); wujiaxi@mail.gyig.ac.cn (J.W.); heyun@mail.gyig.ac.cn (Y.H.); xudan@mail.gyig.ac.cn (D.X.)
[2] School of Geography and Environmental Sciences, Guizhou Normal University, Guiyang 550025, China
[3] College of Resource and Environmental Engineering, Guizhou University, Guiyang 550025, China
[4] College of Eco-Environmental Engineering, Guizhou Minzu University, Guiyang 550025, China
* Correspondence: yanghaiquan@vip.skleg.cn (H.Y.); yyongqiong@163.com (Y.Y.)

Abstract: Combined use of in situ passivation and macrophytes is a valuable technology that exerts remarkable effects on aquatic systems. However, the effectiveness and ecological functions of this combined technology for macrophytes-dominated eutrophic (MDE) lakes with organophosphorus-controlled internal phosphorus (P) loading were poorly understood. In this study, aquatic simulation experiments were performed to study the combination of La-modified materials (LMM; La-modified bentonite (LMB), and La/Al co-modified attapulgite (LAA)) with macrophytes (*Myriophyllum verticillatum* L. (MVL), *Hydrilla verticillata (Linn. f.) royle* (HVR), and *Ceratophyllum demersum* L. (CDL)) for the control of P mobility in the water column, and to investigate the passivator effects on the physiological characteristics of macrophytes. The mineralization of organophosphates (BD−Po, HCl−Po, and Res−Po) is an important factor for maintaining high internal P loadings and overlying water P concentrations in the experiments. Compared with individual treatment groups, the reduction of internal P release flux and porewater SRP concentrations was more obvious in the combined treatments. Moreover, the redox-sensitive P forms transformation is more pronounced in the surface sediments. In the LAA+M group, internal P release flux was reduced by 55% and 55% compared with individual passivators and macrophytes retreatment groups, respectively. In contrast, the LMB+M group decreased by 16% and 46%, respectively. Simultaneously, LMM had less effect on macrophytes traits compared with individual macrophytes group and enhanced the absorption of phosphate by macrophytes. The phosphate content of macrophytes in the LAA+M and LMB+M groups increased by 24% and 11%, respectively, in comparison with the individual macrophytes group. Results concluded that the combination of passivator and macrophytes enhanced the effect of ecological restoration and exerts a synergistic effect on internal P pollution with macrophytes.

Keywords: La-modified material; macrophyte; sediments; phosphorus; eutrophication

1. Introduction

Eutrophication due to excessive enrichment of nutrients such as nitrogen and phosphorus (P) is one of the most important global water quality issues [1,2]. From the perspective of controllability and effectiveness, reducing external and internal P loading has generally been accepted as a key method to mitigate lake eutrophication [3,4]. However, studies have substantiated that the release of P in sediments significantly affected the concentration of P in the lake water as well as the migration and transformation of P at sediment–water interface (SWI) [5,6]. Even when the input of external P is reduced, internal P loading

from sediments may sustain eutrophication in lakes [6,7]. Nevertheless, internal sediment loading remains an important impediment to the restoration and management of aquatic ecosystems within eutrophic lakes.

Effective eutrophication management in macrophytes-dominated lakes requires reduction of external and internal P loading, with reduced internal loading mainly relying on sediments dredging, in situ passivation-based remediation, and aquatic macrophytes community restoration [3,8]. The transition between a clear state in shallow lakes dominated by macrophytes and a turbid state dominated by phytoplankton is very abrupt and difficult to reverse [1,9]. Nutrient reductions alone minimally affect the turbidity of the water column, although appropriate disturbance and ecosystem use may shift the water column to a stable and clear state [3,10]. Further, lakes with high-density macrophytes coverage tend to have a higher clarity than lakes with the same nutrient status but little or no macrophytes coverage [3,9,10]. These observations indicate that constructing a healthy and stable aquatic biological system is key to eutrophication management in macrophyte-dominated lakes.

Aquatic macrophytes community restoration approaches are operationally time-consuming and only slowly achieve pronounced remediation outcomes, while its performance can even be inhibited by continuous high internal loading and seasonal climate change [3,8]. Therefore, improving the physical and chemical conditions of sediments is a necessary measure for water ecological restoration. However, sediments dredging often has problems such as high costs and remediation outcomes, which limit the long-term remediation [11,12]. Therefore, more and more researchers have begun to pay attention to the development of in situ passivation technology. Currently, the passivator for the efficient control of internal P pollution is mainly based on lanthanum-modified materials (LMM), including La-modified bentonite (LMB) [13], La/Al-modified attapulgite (LAA) [14], and La-modified zeolite [15].

The migration and transformation of lake P at SWI are often closely related to the change in different P forms, and the release risk of internal P mainly depends on the forms of P in sediments [16,17]. According to the organophosphorus remineralization and Fe–P coupled pathway of P cycling, sedimentary P dynamics are mainly controlled by depositional flux of organophosphorus and iron-bound P [18,19]. However, a large amount of organophosphorus was often stored in the sediments of macrophytes-dominated lakes due to the strong biological action, and the P cycle may be controlled by microbial decomposition or remineralization [17,20]. Hypoxic diffusion due to enhanced microbial decomposition or remineralization is common in many shallow lakes with high organophosphorus content, and the remediation effects of in situ passivation and macrophytes techniques in these environments are readily affected by sedimentation processes [19,21]. However, ecological remediation effects of in situ passivation and macrophytes techniques on MDE lakes with organophosphorus-dominated internal P loading remain largely unclear. Moreover, changes in microscopic morphology, elemental composition, and surface physical properties of surface sediments in response to the combined use of these techniques also remain unclear.

The objective of this study was to promote the effective application of combined in situ passivator and macrophytes in the MDE lakes with organophosphorus-controlled internal P loading. To this end, a 60-day simulation experiment was conducted to evaluate these aims starting in August 2021 in the heavily polluted areas of Lake Caohai, which is currently experiencing a sudden change in water turbidity, large-scale extinction of macrophytes, and severe eutrophication. Specifically, two highly efficient LMM with three pollution-tolerant, native macrophytes seedlings were used in the experiment. Moreover, the microstructures of sediments before and after sediments remediation were investigated along with the mobility and ecological effects of P in the water column using a combination of modified Hupfer sequential extraction schemes. These measurements were combined with in situ, dynamic, high-resolution composite diffusive gradient in thin films (DGT) technology, scanning electron microscope-X-ray energy dispersive (SEM-EDS) analysis, and X-ray diffraction (XRD) analysis. These results provide a baseline for restoring aquatic

ecosystems in MDE lakes, in addition to evaluating the ecological importance and scientific applicability of LMM.

2. Materials and Methods

2.1. Mesocosm Establishment

The mesocosm experiment was conducted from August to October 2021 at national positioning observation and research station of Caohai wetland ecosystem near Lake Caohai in Weining county, China. Six groups of aquariums were set up (three repetitions): (1) control group without any materials added; (2) macrophytes planted group (M); (3) La/Al co-modified attapulgite added group (LAA); (4) La-modified bentonite group (LMB) added; (5) La/Al co-modified attapulgite added + macrophytes planted group (LAA+M); (6) La-modified bentonite added + macrophytes planted group (LMB+M). Mesocosm experiments were conducted in plexiglass boxes with lengths, width, and height of 40 cm, 40 cm, and 60 cm, respectively. Triplicate parallel samples were used in each group, with nine seedlings planted in each macrophyte's additional group. Dominant macrophytes in seedlings that are native to the lake were used, including three strains *Myriophyllum verticillatum* L. (MVL), *Hydrilla verticillata (Linn. f.) royle* (HVR), and *Ceratophyllum demersum* L. (CDL).

The bottoms of the incubators were lined with mixed homogeneous sediments collected from a heavily polluted area in eastern Lake Caohai to a thickness of 12 cm. Lake water (collected at the Jiangjiawan wharf) was added to the upper layer by the siphon method to achieve a water depth of about 45 cm. All experiment was conducted in the laboratory of the Lake Caohai ecological station. After letting stand for 72 h, two LMM were added (the mass ratio of LMM to biologically available P in the sediments was 100:1), and macrophytes were transplanted. After the start of the experiment, nutrient concentrations in the overlying water of the incubator were regularly measured with the molybdenum blue method (minimum detection limit of 0.01 mg·L^{-1}) [22] and a multiparameter water quality analyzer (YSI EXO-2). Parameters including temperature (T), pH, dissolved oxygen (DO), and oxidation-reduction potential (ORP) were measured on-site in the overlying water. The incubations were conducted for 60-day.

2.2. DGT Deployments and Analysis

Zr-Oxide and AgI DGT probes were vertically inserted as previously described [23] at 30-day and at the end of the incubations. The probes were taken out after letting stand for 24 h. The probes were washed with ultrapure water, sealed, and refrigerated for storage. Additional details regarding the structures and functioning of DGT probes are described elsewhere [24]. The concentrations of unstable elements (C_{DGT}) were calculated as following (Equation (1)):

$$C_{DGT} = \frac{M\Delta g}{DAt} \tag{1}$$

where C_{DGT} is the concentration of the target compound (mg·L^{-1}); M is the accumulated amount of Zr-Oxide DGT thin film over the sampling time (ug); Δg is the thickness of the diffusive layer (cm); D is the molecular diffusive coefficient of the phosphate in the diffusion layer (cm^2·s^{-1}); A is the film area of each slice (cm^2); t is the sample standing time (s) [23].

Both Zr-Oxide (one-dimensional) and AgI DGT (two-dimensional) probes were purchased from Nanjing Zhigan Environmental Technology Co., Ltd. (Nanjing, China). To accomplish two-dimensional high-resolution imaging and vertical profile measurement of DGT-labile S in sediments, the developed AgI-fixed film (600 dpi) images were first converted into grayscale using the CanoScan 5600 F (Canon, Tokyo, Japan) and ImageJ software programs, followed by comparison against a calibration curve. The grey values were then converted into the cumulative mass per unit area (M) of S in the AgI-binding gel using the following Equation (2):

$$M = -7.23 \times ln(\frac{220 - G}{171}) \tag{2}$$

where G is the grayscale intensity of the AgI binding gels. DGT-labile S concentrations could then be calculated from Equation (1).

In order to measure unstable P and Fe concentrations in sediments, the Zr-Oxide fixed film was cut with a razor blade from the exposure window and then sectioned into long strips (with 2 mm width and 20 mm length) with a ceramic microtome. The film was placed in a centrifuge tube with 0.8 mL of 1 M NaOH or 1 M HNO_3 extraction solution and left to stand at room temperature for 16 h for extraction. P and Fe concentrations in the extracts of each section were determined by microplate spectrophotometry with a minimum detection limit of 0.01 mg·L^{-1} and with the concentrations of DGT-labile P and DGT-labile Fe calculated using Equation (1). In order to measure the apparent diffusion flux of P at the WSI in each experimental treatment, Fick's first law of diffusion was used to estimate the specific calculation method [24].

2.3. Sediments Characteristics

After the experiment, sediments (0–8 cm) were collected from each incubator at intervals of 1 cm, followed by cryopreservation. Sediments porewater was obtained by centrifugation at 4000 r/min (MKE-VCK-22R) in the laboratory, and the TP, DIP, and DTP concentrations were measured by the molybdenum blue method [25]. Partial surface sediment samples were used to determine sediments porosity after sediments were freeze-dried (Techconp FD-3-85-MP), and the micro-area surface morphology and mineral compositions were analyzed by scanning electron microscopy (SEM, JEOL, resolution 0.6 nm) and X-ray energy spectroscopy at a resolution of 127.9 eV (EDS, JSM-IT800). The remaining sediment samples were ground and sieved (120 mesh). Followed by sealing for storage. Qualitative phase analysis of sediments was conducted by pre-treating samples (200 mesh), followed by analysis at the Guizhou Provincial Geology and Mineral Centre laboratory. X-ray diffraction instrument (XRD, Rigaku Ultima IV; tube pressure of 40 kV, tube flow of 40 mA; scanning speed of 2°/min) was used for qualitative phase measurements.

The content of sediments TP was determined by the molybdenum blue method after extraction with 3.5 M HCl [25]. The P fraction was obtained using a modified Hupfer sequential extraction method [26], yielding an extraction recovery of >90%. The extracted P forms include weakly adsorbed P (NH$_4$Cl–Pi), iron–manganese-bound inorganic P (BD–Pi), organophosphorus (BD–Po), iron–aluminum-bound inorganic P (NaOH–Pi), biodetritus organophosphorus (NaOH–Po), calcium-bound inorganic P (HCl–Pi), organophosphorus (HCl–Po), residual P (Res–Po) [7,26]. The release or accumulation rates (r) of different P forms during incubation were then estimated using the following formula (3) [27]:

$$r = \frac{P_{60d} - P_{0d}}{P_{0d}} \tag{3}$$

where P_{60d} (mg·kg^{-1}) is the P concentration determined after 60 days of incubation; P_{0d} (mg·kg^{-1}) is the P concentration measured at time zero (before incubation); and r is the proportion of P_{60d} in P_{0d}. Negative values represent reduced P levels over the incubation, indicating release of the fraction, while positive values represent increased P levels over the incubation, indicating accumulation of the fraction.

The release sedimentation rate (R) of P forms in sediments cores was calculated using the method proposed by [28]. The fast-release sedimentation rate (R_1) was calculated from the percentage change in P content of the first and second layers at the top of the columnar sediment, while the slow-release sedimentation rate (R_2) was calculated from the top of the first layer and the bottom of the last layer of the columnar sediment. These measurements were used to calculate the percent change in P concentration as following (Equations (4) and (5)):

$$R_1 = \frac{(S_1 - S_2)}{\sum_{i=1}^{n}|S_1 - S_8|} \times 100\%, \tag{4}$$

$$R_2 = \frac{(S_1 - S_8)}{\sum_{i=1}^{n} |S_1 - S_8|} \times 100\%, \tag{5}$$

where S_1 is the P concentration of the top layer of the columnar sediments; S_2 is the P concentration of the second layer at the top of the columnar sediments; S_8 is the P concentration of the bottom-most layer of the columnar sediments. n represents the number of extracting P forms from sediments. When R_1 and R_2 are positive, that P component is primarily released. When R_1 and R_2 are negative, that P component is primarily retained.

2.4. Macrophytes Traits

Macrophyte growth characteristics (i.e., biomass, length, phosphate content) were measured at the start and end of the experiment. In addition, an additional 10 shoots were selected to measure the water content at the start, which was used to calculate the initial dry weight. All macrophytes were collected, washed three times, and then placed in a 45 °C oven to dry after the experiment. Macrophyte dry weights and lengths were measured with a precision electronic balance and a ruler, respectively. TP content in macrophytes was determined by the molybdenum blue method when macrophytes were extracted with 3.5 M HCl [22]. The relative growth rates (*RGR*) of different macrophytes in the incubator were calculated with the following formula (Equation (6)) [3]:

$$RGR = \ln(\frac{W_{60d}}{W_{0d}})/\text{days}, \tag{6}$$

where W_{60d} (g) and W_{0d} (g) are the total biomass (DW) after 60 day and 0 days of incubation in each incubator, respectively.

3. Results

3.1. Water Quality

LMM and macrophytes, whether used in combination or individually, significantly reduced water column P concentrations (Figures 1 and 2), with the LAA+M group exhibiting the best performance. Aquatic ecosystems in all incubators generally reached steady states by the 15 days of incubation. In addition, SRP concentrations increased after reaching equilibrium stability in all LMM treatments. TP and DTP concentrations were reduced after 60 days of restoration in the M, LAA, LMB, LAA+M, and LMB+M groups by 16% and 30%, 25% and 37%, 33% and 53%, 45%, and 67%, and 38% and 53%, compared with the control group, respectively. In addition, SRP concentrations in the overlying water were below the limit of detection (<0.01 mg·L^{-1}). A comparison of the P removal rates from the water column among treatments indicated that the LMM group was most efficient in controlling water column P concentrations and that its efficiency was further improved when used in conjunction with macrophytes.

The start TP, DTP, and SRP concentrations in surface porewaters before the experiment were 3.80 mg·L^{-1}, 3.09 mg·L^{-1}, and 2.59 mg·L^{-1}, respectively, with SRP accounting for about 68% of TP concentrations. After 30 days of restoration, porewater concentrations of TP, DTP, and SRP were significantly lower than the initial porewater concentrations, while P concentrations were still relatively high in the surface porewater (0–5 cm) of the control group and peak concentrations (TP, DTP, and SRP) were observed at 4 cm depth (Figure 2). Vertical changes of porewater P concentrations in different treatment groups were basically the same as those of the control group, and the peak concentrations occurred at deeper depths in the LAA+M (5 cm) and LMB+M (6 cm) groups. All of the treatments, except for the LAA+M and LMB+M groups, did not show significant changes in porewater P concentrations at the end of the experiment compared with the initial porewater P concentrations. Further, SRP was the dominant porewater P form among profiles, accounting for about 47% of TP concentrations and about 71% of DTP concentrations. The LAA+M group achieved the best restoration outcome, with porewater

concentrations of TP, DTP, and SRP decreasing by 53%, 53%, and 62%, compared with the control group, respectively.
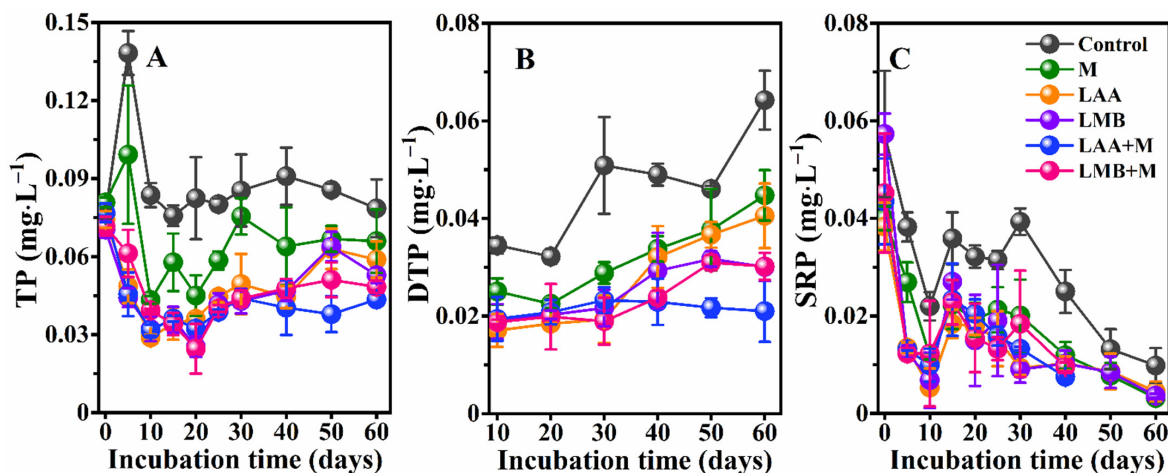

Figure 1. The changes of TP, DTP, and SRP concentrations in the overlying water of the six treatments during the experiment. Vertical bars indicate standard deviation. (**A**–**C**) represent TP, DTP, and SRP in the overlying water, respectively.
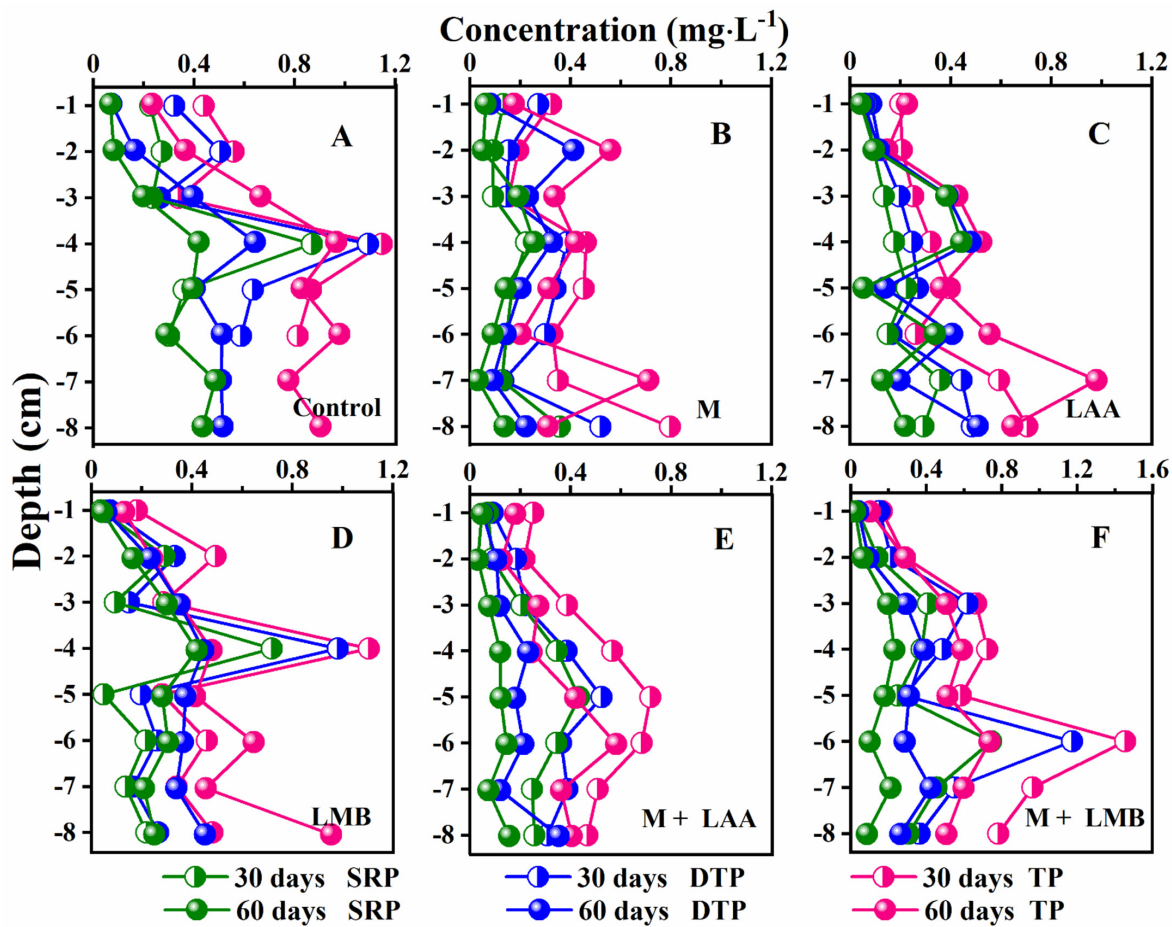

Figure 2. The changes of TP, DTP, and SRP concentrations in the porewater of the six treatments during the experiment. All data are triplicates. (**A**–**F**) indicate the concentration changes of TP, DTP, and SRP in sediment pore water of the Control, M, LAA, LMB, LAA+M, and LMB+M experimental groups on the 30-day and 60-day, respectively.

3.2. Physicochemical Characterization of Sediments

SEM-EDS elemental mapping revealed that C, O, Si, Al, and Ca are the primary chemical elements in Lake Caohai sediments, and $CaCO_3$ and SiO_2 are the main minerals in the sediments (Figure 3A,E). SEM imaging revealed that minerals in the surface sediments were in crystal form, ranging from 1 to 10 μm in size (Figure 3C,F). Surface sediments treated with LMM passivators exhibited significantly higher content of La^{3+} compared with the control sediments (Figure 3B,C,F,G) owing to the high dosage used in the preparation of LMM (Figure 3D,H).
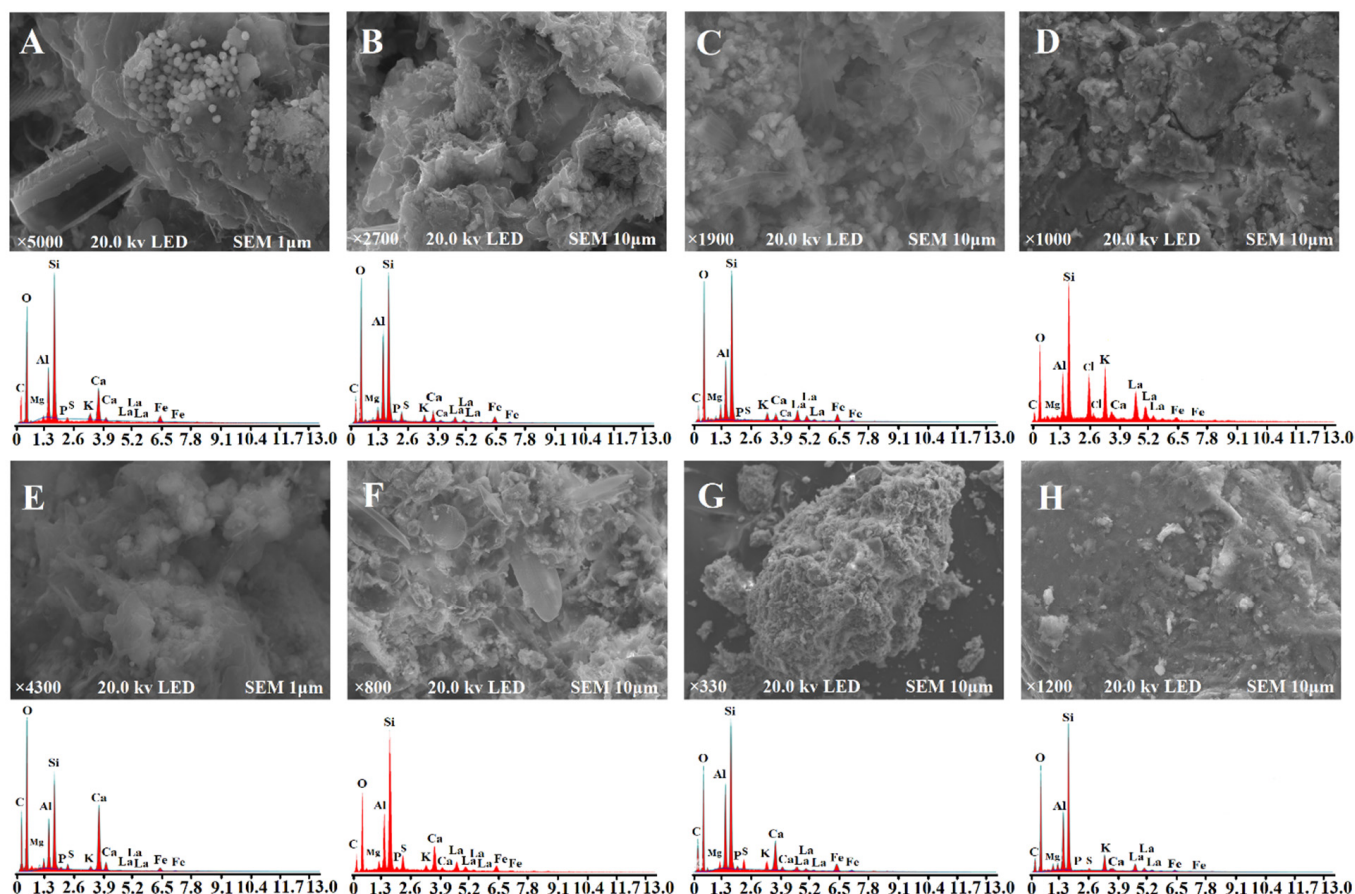
Figure 3. SEM images and spectra of chemical composition of Control (**A**), LAA (**B**), LAA+M (**C**), Original LAA (**D**), M (**E**), LMB (**F**), LMB+M (**G**) and Original LMB (**H**). Original LAA and Original LMB are substances that are not mixed with sediments respectively.

XRD peak positions exhibited large differences between LMM treatment profiles and those from other treatment groups (Figure 4). Bragg equation and Scherrer formula calculations revealed a lack of changes in the characteristic peak position and d-values of LMM-treated surface sediments compared with those from the control group, indicating that moderate LMM exposure would not change the crystalline structure of original lake sediments but would reduce sediments grain sizes (Table S1). Quantitative analysis also revealed that the LMM group did not lead to changes in the basic mineral composition of the original lake sediments (taranakite) but led to a sharp decrease in $Ca(PO_3)_2$ mass fractions (Table 1).
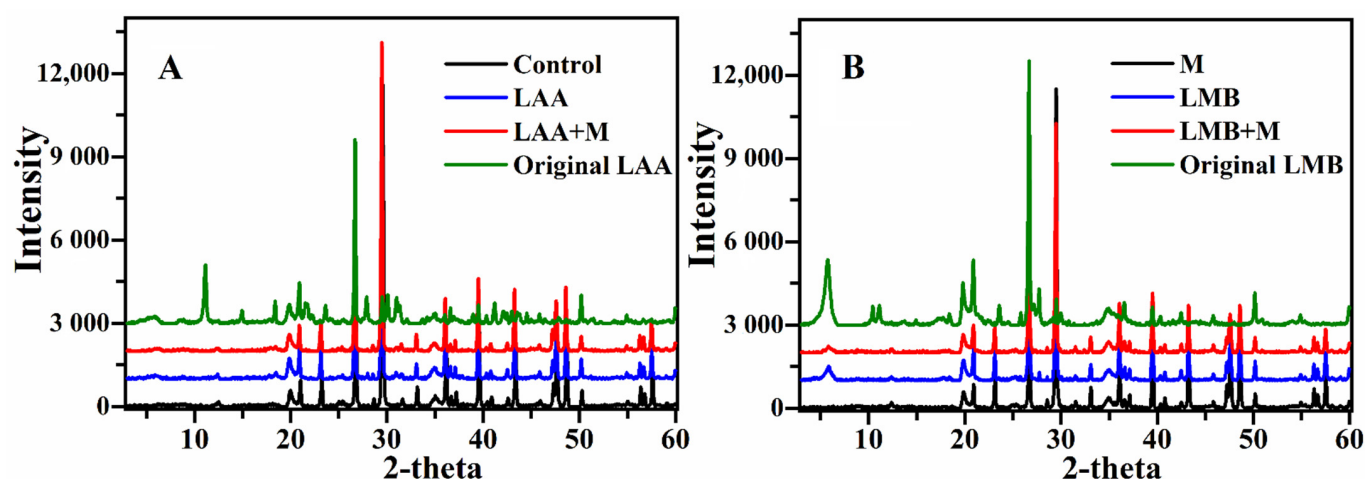
Figure 4. (**A**) statistical XRD patterns of control, LAA, LAA+M, and Original LAA. (**B**) statistical XRD patterns of M, LMB, LMB+M, and Original LMB. Original LAA and Original LMB are substances that are not mixed with sediments respectively.

Table 1. Chemical composition (mass fraction) of surface sediments after restoration experiments.

Material	Control	M	LAA	LMB	LAA+M	LMB+M
$CaCO_3$	55.6%	57.8%	45.5%	46.1%	58.6%	46.3%
SiO_2	18.1%	18.0%	22.0%	25.6%	19.2%	24.0%
$K_{0.77}Al_{1.93}(Al_{0.5}Si_{3.5})O_{10}(OH)_2$	15.7%	14.1%	19.5%	19.4%	13.9%	16.7%
$Al_2(Si_2O_5)(OH)_4$	6.0%	4.7%	7.8%	4.9%	3.6%	3.4%
FeS_2	3.1%	3.3%	2.4%	2.6%	2.9%	2.7%
$Ca(PO_3)_2$	1.4%	2.2%	1.0%	1.6%	0.5%	0.9%

3.3. Sediments P

Sediments TP concentrations ranged from 572.7 to 927.2 mg·kg^{-1}, with a mean of 733.7 ± 86.0 mg·kg^{-1}, which is indicative of moderate pollution levels (Figure S1A), and that is generally consistent with those measured in a recent study [17]. Sediments P primarily existed in the following inorganic (Pi) and organic (Po) forms, NaOH–Pi, HCl−Pi, BD–Po, NaOH–Po, and Res–Po, with mean concentrations of 174.4 ± 31.5 mg·kg^{-1}, 99.8 ± 16.0 mg·kg^{-1}, 91.0 ± 34.6 mg·kg^{-1}, 115.4 ± 45.3 mg·kg^{-1}, and 121.0 ± 14.5 mg·kg^{-1}, respectively (Figure 5 and Figure S2). The eight extractable forms of sediments P exhibited varying degrees of transport and transformation during the incubation period. After 60 days of restoration, the concentrations of BD–Pi, NaOH–Pi, NaOH–Po, HCl–Pi, HCl–Po, and Res–Po in the water column increased by 7%, 52%, 40%, 3%, 11%, and 23%, compared with concentrations before the restoration, respectively, while NH_4Cl–Pi and BD–Po concentrations decreased by 63% and 43%, respectively.

The NaOH–Pi concentrations of sediments cores were significantly lower in each treatment than in the control group, while the HCl–Po concentrations were significantly higher. The BD–Po, BD–Pi, and NaOH–Pi concentrations in all LMM-treated sediments gradually increased with increasing depth, while the NaOH–Po, HCl–Pi, and HCl–Po concentrations decreased with depth. In addition, the vertical profile of BD–Po concentrations in sediments subjected to combined treatments significantly differed from those in other sediments, with the means of both R_1 and R_2 being negative for the combined treatment sediments. Moreover, the vertical sediment profiles of each P form indicated that the low P concentrations of bottom sediments were primarily due to decreased concentrations of BD–Po, NaOH–Po, and HCl–Pi that exhibited average R_2 values after 60 days of restoration of 10%, 13%, and 11%, respectively.
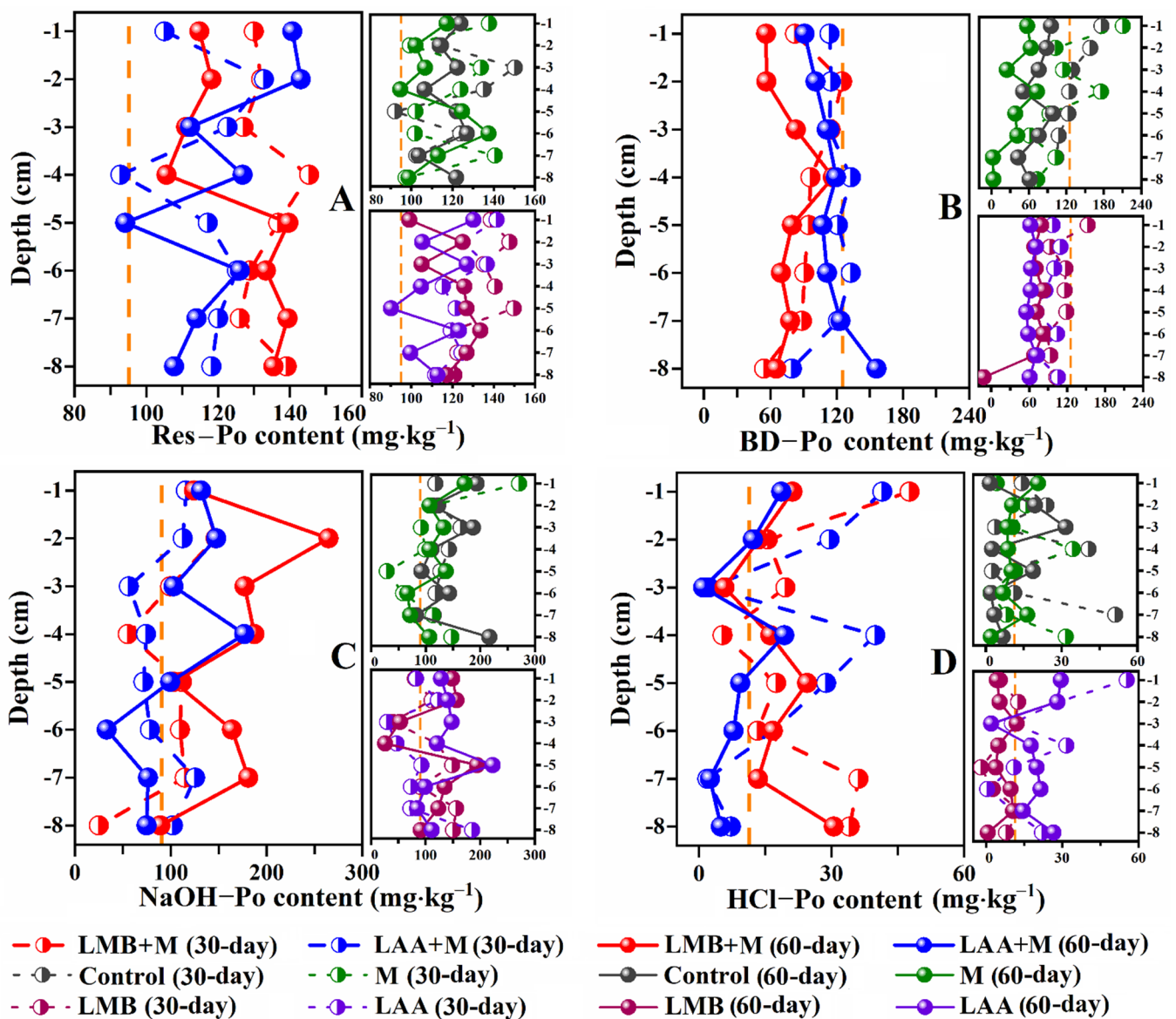
Figure 5. Vertical distribution of different P forms in sediments of the six treatment groups during the experiment. (**A**–**D**) represent the changes of Res−Po, BD−Po, NaOH−Po and HCl−Po contents in sediment, respectively. Each graph consists of three distinct subgraphs. The left subgraphs represent LAA+M and LMB+M groups, respectively. The upper right subgraphs represent control and M groups, respectively. The lower right subgraphs represent LAA and LMB groups, respectively. All data are triplicates. The vertical dashed line is the start P contents of the sediments.

3.4. DGT-Labile P, Fe, and S Variation

The one-dimensional distribution of DGT-labile P, Fe, and S is shown in Figure 6, with concentrations ranging from 0.01 to 0.63 mg·L^{-1}, 0.01 to 1.76 mg·L^{-1}, and 0.01 to 0.89 mg·L^{-1}, respectively. DGT-labile P, Fe, and S concentrations in the water column were about 3, 20, and 2 times higher than in the overlying water after 60 days of restoration. Overall, DGT-labile P/Fe/S concentrations in each group first increased and then stabilized or decreased with increasing depth (Figure S3). High correlations were observed for DGT-labile P concentrations and DGT-labile S concentrations along water columns, with linear correlation coefficients of >0.77 for all treatments, with the exception of the M group ($R^2 = 0.40$). The DGT-labile Fe concentrations considerably varied vertically and peaked in the top sediment layers of all experimental groups, exhibiting an increasing trend with incubation time that was most significant in the control and M groups. However, the linear

correlation of DGT-labile Fe concentrations was minimal with respect to DGT-labile P and DGT-labile S concentrations (Table 2).
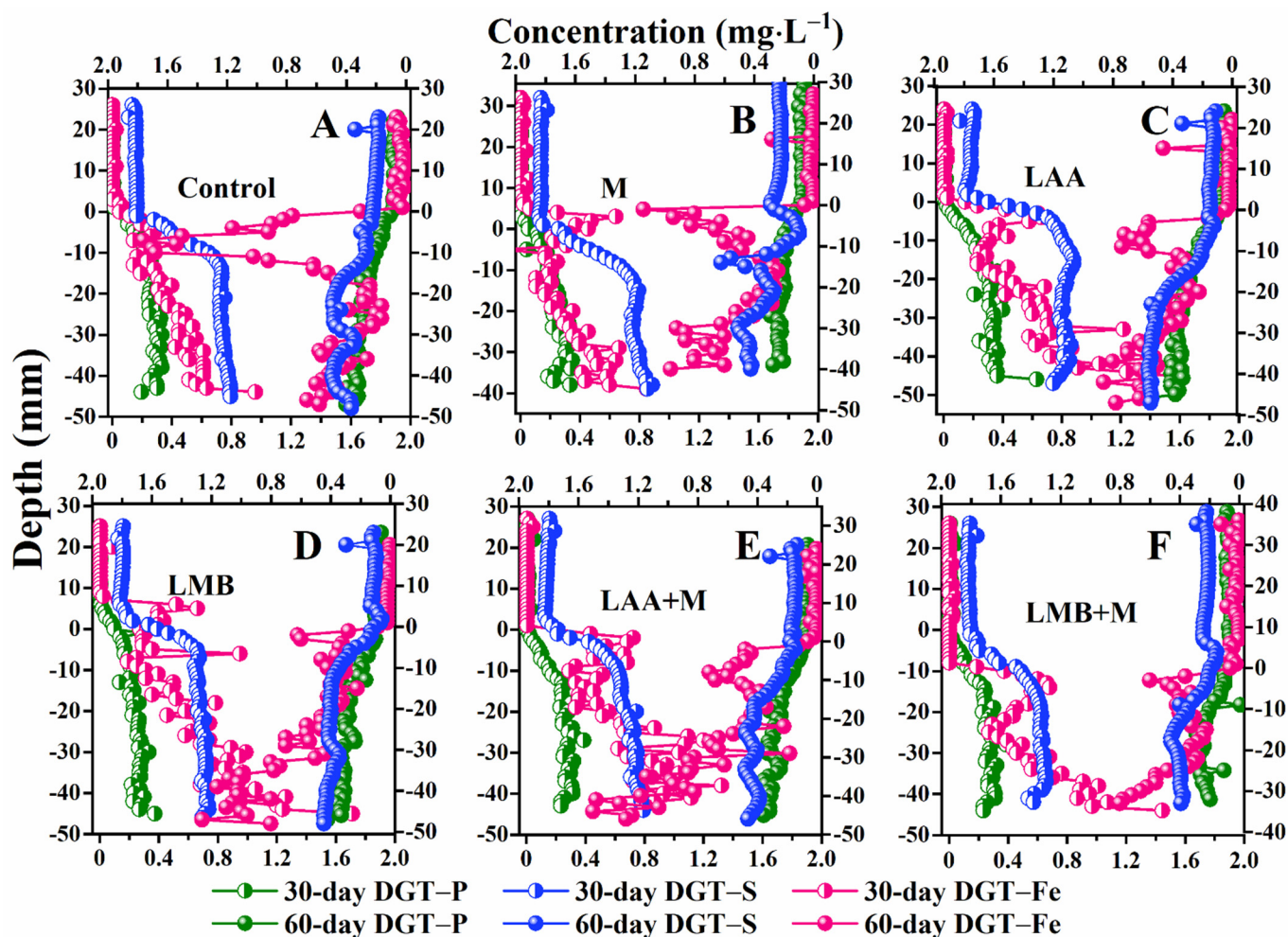
Figure 6. Vertical change of the DGT-labile P (Fe/S) concentrations in sediments of the six treatments groups during the experiment. The location of the sediment–water interface is represented by zero. (**A–F**) indicate the changes of DGT-labile P (Fe/S) concentrations in sediment of the Control, M, LAA, LMB, LAA+M, and LMB+M groups on the 30-day and 60-day, respectively.

Table 2. Relationships between DGT-labile P, DGT-labile Fe, and DGT-labile S ($p < 0.05$) in sediments of the six treatments used in the experiment.

Sample	30-Day			60-Day		
	P/Fe	P/S	Fe/S	P/Fe	P/S	Fe/S
Control	0.76	0.95	0.78	0.08	0.79	0.01
M	0.55	0.91	0.43	0.48	0.41	0.13
LAA	0.66	0.77	0.58	0.58	0.83	0.42
LMB	0.67	0.91	0.57	0.70	0.86	0.60
LAA+M	0.73	0.91	0.77	0.64	0.86	0.54
LMB+M	0.66	0.93	0.75	0.38	0.77	0.43

The internal flux of DGT-labile P at SWI was calculated based on Fick's first law of diffusion and was estimated to range from 0.28 to 0.95 mg·m^{-2}·d^{-1} during the 30 days and 60 days of restoration (Table 3). At the end of the experiment, the internal flux of DGT-labile P was lower to different degrees in all experimental groups compared with flux on the 30-day. This was particularly evident in the LAA+M group, which exhibited the

lowest internal flux of 0.28 mg·m^{-2}·d^{-1} representing 60% and 44% lower levels than in the control group on the 30-day and in the LAA+M group at the beginning of the experiment, respectively. In contrast, the internal flux of DTG-labile P was 0.63 mg·m^{-2}·d^{-1}, 0.63 mg·m^{-2}·d^{-1}, 0.41 mg·m^{-2}·d^{-1}, and 0.34 mg·m^{-2}·d^{-1} in the M, LAA, LMB, and LMB+M groups, respectively.

Table 3. The apparent diffusion fluxes of P (mg·m^{-2}·d^{-1}) at sediment–water interfaces among different experimental treatments.

Time	Control	M	LAA	LMB	LAA+M	LMB+M
30-day	0.95	0.68	0.77	0.86	0.50	0.40
60-day	0.70	0.63	0.63	0.41	0.28	0.34

3.5. Macrophytes

The TP contents of macrophyte seedlings in the M, LAA+M, and LMB+M groups increased by 41%, 71%, and 57% during the incubation period, respectively (Figure 7A). The mean net height growth of seedlings was 98 cm, 58 cm, and 10 cm in the MVL, HVR, and CDL treatments, respectively (Figure 7B), with mean *RGR* values of 0.02 d^{-1}, 0.03 d^{-1}, and 0.004 d^{-1}, respectively (Figure 7C).
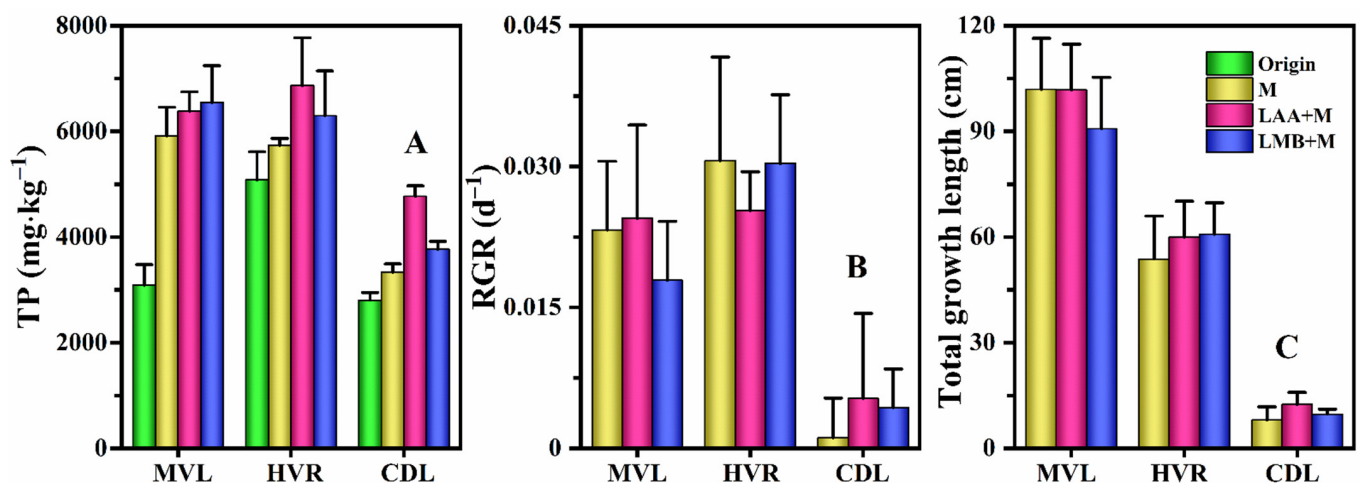
Figure 7. Macrophyte traits at the experiment. (**A**) indicates the change of TP content in different types of macrophytes. (**B,C**) represent the relative growth rate (*RGR*) and total growth length (length of macrophyte growth between the start and end of the experiment) of macrophytes in the experiments, respectively. MVL, HVR and CDL are *Myriophyllum verticillatum* L., *Hydrilla verticillata (Linn. f.) royle* and *Ceratophyllum demersum* L., respectively.

4. Discussion

4.1. Effects of LMM and Macrophytes on P Concentrations

The TP concentrations in overlying waters in the M, LAA, LMB, LAA+M, and LMB+M groups decreased by 28%, 48%, 51%, 55%, and 51% over the experimental period compared with the control group, respectively (Figure 1). Thus, combined treatment with both LMM and macrophytes led to better restoration performance of lake water P than individual treatments with LMM or macrophytes. However, the combined effects were not a simple summation of the two separate effects [3,13]. Changes in P concentrations in the overlying water indicated that the two restoration methods, whether used alone or in combination, primarily removed SRP fractions from the water column. SRP removal rates exceeded 88% in all treatment groups by the 60 days of restoration, while dissolved organophosphorus (DOP) and particulate P (PP) generally increased after stabilization of water quality in the incubators.

Combined treatment with both LMM and macrophytes effectively inhibited the release of P from sediments. Indeed, the diffusion fluxes of P in the water column after 60-day were reduced by 55% and 55% in the LAA+M group compared with the LAA and M groups, respectively, and by 16% and 46% in the LMB+M group compared with the LMB and M groups, respectively (Table 3). Consequently, both restoration methods, whether used alone or in combination, can reduce internal P loading in lakes, although combined use leads to better performance. In addition, changes in porewater P concentrations among different experimental groups indicated that the combined treatment was more effective in removing P from water columns. Between the 30 days of incubation and the end of the experiment, porewater TP concentrations decreased by 33% and 27% in the LAA+M and LMB+M groups, respectively, but increased by 34%, 13%, and 28% in the LAA, LMB, and M groups, respectively (Figure 2).

High internal P loading in the water column and high aqueous P concentrations was maintained owing to the transport and transformation of NH_4Cl–P, BD–Pi, BD–Po, and Res–Po during the experiment. The mean accumulation rates (*r*) of these P forms were negative for most sediments cores during the incubation period, indicating that these forms mostly entered the overlying water through mineralization, degradation, resuspension, or gradually transformed into more stable forms, such as NaOH–Pi, NaOH–Po, HCl–Pi, and HCl–Po (Table S2) [27]. The accumulation or release of different P forms in sediments cores over the incubation period was also investigated. These analyses revealed that (1) sediment accumulation of NaOH–Pi, NaOH–Po, and HCl–Pi was higher in the LAA+M and LMB+M groups than in other groups over the incubation period; (2) the release of redox-sensitive BD–P (comprising BD–Pi and BD–Po) was higher in the LAA (61.6 mg·kg^{-1}), LMB (63.3 mg·kg^{-1}), and M (82.2 mg·kg^{-1}) groups than in the other treatment groups; and (3) total P accumulation was greater than total P release in the combined treatment groups, while the opposite was observed in the individual treatment groups. These phenomena may be attributed to oxygen transfer from roots to rhizosphere sediments during the growth of macrophytes, the mineralization of organophosphate, and the strong ability of La to bind P [14,29,30]. In particular, oxygen release from macrophytes roots can cause oxidation of compounds in rhizospheres such as low-valence Fe, Mn, and other metals to generate high-valence P-containing compounds, thereby leading to the continuous accumulation of P [17,31]. Further, organophosphorus mineralization also results in changes to redox conditions and pH that, in turn, affect the transport and transformation of BD–TP and NaOH–Pi in sediments [21,27]. Increased HCl–P concentrations (i.e., the sum of HCl–Pi and HCl–Po) in the sediments may be related to the generation of $LaPO_4$(s) that primarily exists as HCl–P when extracted with HCl [14,32].

4.2. Effects of LMM on Macrophytes Physiological Indices

The root systems of macrophytes are the primary area where biologically available P (BAP, comprising NH_4Cl–Pi, BD–Pi, NaOH–Pi, and HCl–Pi) is taken up from surface sediments. Thus, the reduction in sediments BAP concentrations due to the addition of LMM may negatively affect macrophyte growth [3,33]. Experimental studies have documented species-specific differences in the effects of LMM on macrophytes species [34–36], consistent with the results of this study, wherein the net height growth of the macrophytes HVR and CDL, in addition to the *RGR* of HVR, were slightly higher in the combined treatments than individual macrophytes treatments (Figure 7B,C). However, LMM addition to a 100:1 mass ratio in this study led to a low inhibitory effect on the growth of macrophytes. Differences in net height growth and the *RGR* between groups treated with individual macrophytes and combined treatments were small, likely because LMM passivation provided suitable environments but also contributed nutrients such as K and Mg that could support the growth of macrophytes (Figure 3D,F). The BAP concentrations of surface sediments on the 30 days of restoration were significantly higher in the treatments with individual macrophytes than in the LMM treatments, while the opposite was observed at the end of the experiment (Figure S1B). Further, the phosphate concentrations of macrophytes in the combined treat-

ments were significantly higher by 24% and 11% than in the treatments with individual macrophytes, respectively (Figure 7A). Thus, insignificant passivation at the early stage of restoration led to slow macrophytes germination and growth in the lake ecosystem, while improved water quality in the middle and later stages promoted macrophytes growth, as demonstrated by differences in porewater TP concentrations between different treatment groups (Figure 2). Overall, LMM addition to a 100:1 mass ratio led to minimal negative effects on macrophytes growth.

4.3. Effects of LMM on Surface Sediments Microenvironment

Ultra-high-resolution SEM-EDS imaging and XRD spectroscopy further revealed changes in the microscopic morphologies and structures of remediating sediments in response to combined treatment with both in situ adsorption and biological forcing. SEM-EDS elemental mapping revealed that La–P minerals were predominantly present as sub-nanometre crystals in surface sediments (Figure 3B–D,F). Further, the high Si, Ca, and O elemental ratios in sediments indicated strong chemical weathering in the source area that would lead to the dissolution of phosphate-bearing minerals and phosphate release. XRD analysis also revealed that surface sediments phosphate primarily existed as taranakite, while LMM resulted in a significant decrease in the mass fraction of taranakite and $Ca(PO_3)_2$ during restoration (Table 1). Nevertheless, macrophytes enhanced the FeS_2 and $CaCO_3$ mass fractions in the surface sediments.

The concentration difference between sediments porewater and overlying water in lake systems is an important factor driving internal P release in lakes [4,17]. Due to the obvious differences between passivation materials and lake sediments in the microscopic morphology, elemental composition, and surface physical properties, the addition of LMM will change the physical and chemical properties of the surface sediments. Numerous studies have shown that the structure collapse and pore blockage caused by LMB and LAA increase the specific surface areas of the passivation materials and the adsorption capacity for phosphate during the high temperature of calcination, and the static layer formed at SWI is the key to maintaining the repair of LMM [14,32]. SEM-EDS elemental mapping revealed that LMB and LAA materials were composed of nanosheet aggregates of various sizes and contain metallic elements such as Al^{3+}, K^+, Ca^{2+}, and La^{3+} (Figure 3D,H). The modified bentonite and attapulgite have a large number of positive charges on the surface, which helps LMM to have a strong adsorption effect on P and algae [8,14]. This may be an important reason why NaOH–P and HCl–P contents different at different deposition depths in the surface sediments of the LMM treatment groups were significantly higher than that of other treatment groups. According to changes in P forms content, the redox-sensitive P forms (NH_4Cl–P and BD–P) mainly migrate to NaOH–P and HCl–P in the surface sediments, indicating that LMM can lead to the migration and transformation of redox-sensitive chemical forms at SWI. Combined with the release flux characteristics of P in the sediment profiles, it was shown that LMM-induced changes in the surface sediments microenvironment also affect the decay or release rates of P in lake systems, although it is usually limited by the stable performance of a static layer a few millimeters on top of the sediments.

4.4. P Biogeochemical Behaviour

The transport and transformation of P at SWI are primarily controlled by the stability of different P forms and various physical, geochemical, and biological processes [18,37]. The inorganic P forms of NH_4Cl–P, BD–Pi, NaOH–Pi, and HCl–Pi are considered unstable P fractions (BAP) in the modified Hupfer sequential extraction scheme and are easily released from the solid phase to the aqueous phase under certain conditions [26,38,39]. In the present study, the mean BAP to TP ratios in sediments cores after 60 days of restoration were 53%, 50%, 47%, and 51% in the LMA, LMB, LAA+M, and LMB+M groups, respectively, indicating that the P fractions in the water column are unstable when LMM are used to remediate sediments [14,32].

Evaluation of the sedimentation rates (R) of P fractions in sediments cores (Tables S3 and S4) revealed that organophosphorus mineralization is the main internal source of P in all of the LMM-treated sediments [28,40]. Although high BAP concentrations and internal P fluxes were observed in the sediments, the geochemical reactions dominated by the reduction and dissolution of P-iron oxides/hydroxides contribute little to overlying water P concentrations in macrophyte-dominated lakes because these lakes are characterized by high DO concentrations and high reduction potential (Figure S4B,D). These dynamics are further substantiated by the non-significant linear correlation between water column DGT-labile P and DGT-labile Fe during the experiment (Table 2). Further, the significant positive correlation observed between DGT-labile P and DGT-labile S was consistent with the observation that the refractory P fractions in sediments (e.g., NaOH–Po, HCl–Pi, and HCl–Po) exhibited positive release and sedimentation rates (R) since high sulfate concentrations would lead to the reductive release of some insoluble phosphates from sediments [41,42].

The concentrations of various P forms were also analyzed. The free phosphate ions released in the LMM treatment groups were primarily adsorbed by La^{3+} to form La-phosphate compounds ($LaPO_4 \cdot nH_2O$) [14,15], as confirmed by EDS spectroscopy (Figure 3B–D,F). These observations correspond to high La^{3+} concentrations in LMM and because La^{3+} exhibits stronger electronegativity than other metal ions such as Fe and Al. The mass fraction of FeS_2 in different experimental groups, the transport and transformation characteristics of P in sediments profiles, and DGT-labile Fe concentration trends in sediments cores jointly suggested that the dissimilatory reduction of Fe in macrophytes roots may be an important pathway for organic matter metabolism in surface sediments [43,44].

BD–Po and NaOH–Po are reactive organophosphate forms that can be mineralized and hydrolysis under certain conditions, leading to dissolving phosphate or small organophosphate compounds that can be easily absorbed and used by organisms [26,45]. HCl–P and Res-Po are stable forms and will be released under strongly acidic or alkaline conditions to some extent [6,46]. All forms of sediments P in each treatment group in this study, except the HCl–P and Res–Po forms, exhibited decreased concentrations across the incubation period compared with the control group (Table S5). This observation, when combined with the transport and transformation characteristics of P in the sediments (Table S2) and the XRD analyses, indicated that the active ingredient in the Supplemented Material reacted with P compounds in the sediments through ligand exchange, electrostatic interaction, and Lew is acid–base interaction to form stable La–P minerals ($LaPO_4 \cdot nH_2O$) [47,48]. Further analysis revealed that BD–Po and NaOH–Po concentrations in the 0–1 cm sediment layer were significantly lower in all treatments than in the control group. This was especially evident in the LAA+M group, where BD–Po and NaOH–Po concentrations on the 60-day were lower by 40% and 11% compared with the control, respectively, which may be related to the microbial decomposition of organophosphate. These results were consistent with the SEM-EDS imaging that revealed dentate flocs (Figure 3C,F) resembling microorganisms that have been previously reported [49,50]. Nevertheless, the short incubation period used in the present study may fail to reveal the possible inter-annual or monthly variation of macrophytes when this technique is applied in real-world scenarios. Therefore, long-term monitoring of changes in MDE lakes in response to the combined application of LMM and macrophytes is needed.

5. Conclusions

In this study, a practical approach for efficient ecological restoration is described for MDE lakes with organophosphorus-controlled internal P loading. The results indicate that mineralization of organophosphates (BD–Po, HCl–Po, and Res–Po) is an important factor for maintaining high internal P loadings and overlying water P concentrations during the experiments. The combination of LMM and macrophytes led to synergistic effects in the performance of aquatic ecological restoration compared with individual retreatments. Specifically, the combined treatments exhibited lower internal P loading than individual

treatments. This was especially evident for the LAA+M group that achieved the best restoration outcome. SEM-EDS elemental mapping and XRD analysis revealed that the active ingredient in the added material reacted with sediments P forms to form stable La–P compounds ($LaPO_4 \cdot nH_2O$). LMM also enhanced the conversion rates of redox-sensitive P forms in surface sediments. Simultaneously, LMM had less effect on macrophyte traits (e.g., relative growth rate (*RGR*), length) compared with individual macrophyte groups and enhanced the absorption capacity of phosphate by macrophytes.

Supplementary Materials: The following supporting information can be downloaded at: https://www.mdpi.com/article/10.3390/w14121847/s1, Table S1. The 2θ, interlayer spacing (d) and crystal size (CS) of different experimental groups in the experiment; Table S2. The release and accumulation rates (r) of P in sediments cores during the experiment; Table S3. The fast-release and sedimentation rates (R1) of different P forms in sediments cores during the experiment; Table S4. The flow-release and sedimentation rates (R2) of different P forms in sediments cores during the experiment; Table S5. The increase or decrease rates of different P forms in the sediment cores of different treatment groups relative to the control group during the experiment; Figure S1. Vertical distribution of P content in the sediments of the different treatments during the experiment. (A–C) represent the content changes of TP, Pi, and Po in the sediments, and each graph consists of three distinct subgraphs. The left subgraphs represent LAA+M and LMB+M groups, respectively. The upper right subgraphs represent control and M groups, respectively. The lower right subgraphs represent LAA and LMB groups, respectively. All data are three replicates; Figure S2. Vertical distribution of P content in sediments of different treatments during the ex-periment. (A–D) represent the changes in the content of inorganic NH4Cl-P, BD-Pi, NaOH-Pi and HCl-Pi in the sediments, respectively. Each graph consists of three distinct subgraphs. The left subgraphs represent LAA+M and LMB+M groups, respectively. The upper right subgraphs represent control and M groups, respectively. The lower right subgraphs represent LAA and LMB groups, respectively. All data are triplicates. The vertical dashed line is the initial P content of the sediments; Figure S3. Vertical variation of DGT-labile S in sediments during the experiment. (A–F) are the changes of DGT-labile S in the sediments of the Control, M, LAA, LMB, LAA+M and LMB+M repaired on the 30-day, respectively. (A1), (B1), (C1), (D1), (E1), and (F1) are the changes of DGT-labile S in the sediments of the Control, M, LAA, LMB, LAA+M and LMB+M re-paired on the 60-day, respectively; Figure S4. Water quality parameters. (A–D) respectively represent the overlying water temperature (T), dissolved oxygen (DO), pH and redox potential (ORP) changes during the experiment.

References

1. Smith, V.H.; Schindler, D.W. Eutrophication science: Where do we go from here? *Trends Ecol. Evol.* **2009**, *24*, 201–207. [CrossRef] [PubMed]
2. Oosterhout, F.V.; Waajen, G.; Yasseri, S.; Manzi Marinho, M.; Pessoa Noyma, N.; Mucci, M.; Douglas, G.; Lürling, M. Lanthanum in Water, Sediment, Macrophytes and chironomid larvae following application of Lanthanum modified bentonite to lake Rauwbraken (The Netherlands). *Sci. Total Environ.* **2020**, *706*, 135188. [CrossRef] [PubMed]
3. Zhang, X.M.; Zhen, W.; Jensen, H.S.; Reitzel, K.; Jeppesen, E.; Liu, Z.W. The combined effects of macrophytes (Vallisneria denseserrulata) and a lanthanum-modified bentonite on water quality of shallow eutrophic lakes: A mesocosm study. *Environ. Pollut.* **2021**, *277*, 116720. [CrossRef] [PubMed]
4. Tammeorg, O.; Nürnberg, G.; Horppila, J.; Haldna, M.; Niemistö, J. Redox-related release of phosphorus from sediments in large and shallow Lake Peipsi: Evidence from sediment studies and long-term monitoring data. *J. Great Lakes Res.* **2020**, *46*, 1595–1603. [CrossRef]
5. Recknagel, F.; Hosomi, M.; Fukushima, T.; Kong, D.S. Short- and long-term control of external and internal phosphorus loads in lakes—A scenario analysis. *Water Res.* **1995**, *29*, 1767–1779. [CrossRef]
6. Wang, Y.T.; Zhang, T.Q.; Zhao, Y.C.; Ciborowski, J.J.H.; Zhao, Y.M.; O'Halloran, I.P.; Qi, Z.M.; Tan, C.S. Characterization of sedimentary phosphorus in Lake Erie and on-site quantification of internal phosphorus loading. *Water Res.* **2021**, *188*, 116525. [CrossRef]
7. Zhang, R.Y.; Wang, L.Y.; Wu, F.C.; Song, B.A. Phosphorus speciation in the sediment profile of Lake Erhai, southwestern China: Fractionation and ^{31}P NMR. *J. Environ. Sci.* **2013**, *25*, 1124–1130. [CrossRef]
8. Waajen, G.; Pauwels, M.; Lürling, M. Effects of combined flocculant–Lanthanum modified bentonite treatment on aquatic macroinvertebrate fauna. *Water Res.* **2017**, *122*, 183–193. [CrossRef]
9. Hilt, S.; Gross, E.M. Can allelopathically active submerged macrophytes stabilise clear-water states in shallow lakes? *Basic Appl. Ecol.* **2008**, *9*, 422–432. [CrossRef]
10. Scheffer, M.; Hosper, S.H.; Meijer, M.L.; Moss, B.; Jeppesen, E. Alternative Equilibria in Shallow Lakes. *Trends Ecol. Evol.* **1993**, *8*, 275–279. [CrossRef]
11. Fathollahzadeh, H.; Kaczala, F.; Bhatnagar, A.; Hogland, W. Significance of environmental dredging on metal mobility from contaminated sediments in the Oskarshamn Harbor, Sweden. *Chemosphere* **2015**, *119*, 445–451. [CrossRef] [PubMed]
12. Yin, H.; Yang, C.; Yang, P.; Kaksonen, A.H.; Douglas, G.B. Contrasting effects and mode of dredging and in situ adsorbent amendment for the control of sediment internal phosphorus loading in eutrophic lakes. *Water Res.* **2020**, *189*, 116644. [CrossRef] [PubMed]
13. Lin, J.W.; Zhao, Y.Y.; Zhan, Y.H.; Wang, Y. Control of internal phosphorus release from sediments using magnetic lanthanum/iron-modified bentonite as active capping material. *Environ. Pollut.* **2020**, *264*, 114809. [CrossRef] [PubMed]
14. Yin, H.B.; Yang, P.; Kong, M.; Li, W. Use of lanthanum/aluminum co-modified granulated attapulgite clay as a novel phosphorus (P) sorbent to immobilize P and stabilize surface sediment in shallow eutrophic lakes. *Chem. Eng. J.* **2020**, *385*, 123395. [CrossRef]
15. Goscianska, J.; Ptaszkowska-Koniarz, M.; Frankowski, M.; Franus, M.; Panek, R.; Franus, W. Removal of phosphate from water by lanthanum-modified zeolites obtained from fly ash. *J. Colloid Interface Sci.* **2018**, *513*, 72–81. [CrossRef]
16. Xiang, S.L.; Zhou, W.B. Phosphorus forms and distribution in the sediments of Poyang Lake, China. *Int. J. Sediment Res.* **2011**, *26*, 230–238. [CrossRef]
17. Yu, W.; Yang, H.Q.; Chen, J.A.; Liao, P.; Chen, Q.; Yang, Y.Q.; Liu, Y. Organic Phosphorus Mineralization Dominates the Release of Internal Phosphorus in a Macrophyte-Dominated Eutrophication Lake. *Front. Environ. Sci.* **2022**, *9*, 812834. [CrossRef]
18. Barik, S.K.; Bramha, S.; Bastia, T.K.; Behera, D.; Kumar, M.; Mohanty, P.K.; Rath, P. Characteristics of geochemical fractions of phosphorus and its bioavailability in sediments of a largest brackish water lake, South Asia. *Ecohydrol. Hydrobiol.* **2019**, *19*, 370–382. [CrossRef]
19. Joshi, S.R.; Kukkadapu, R.K.; Burdige, D.J.; Bowden, M.E.; Sparks, D.L.; Jaisi, D.P. Organic matter remineralization predominates phosphorus cycling in the mid-Bay sediments in the Chesapeake Bay. *Environ. Sci. Technol.* **2015**, *49*, 5887–5896. [CrossRef]
20. Zhu, Y.R.; Feng, W.Y.; Liu, S.S.; He, Z.Q.; Zhao, X.L.; Liu, Y.; Guo, J.Y.; Giesy, J.P.; Wu, F.C. Bioavailability and preservation of organic phosphorus in lake sediments: Insights from enzymatic hydrolysis and ^{31}P nuclear magnetic resonance. *Chemosphere* **2018**, *211*, 50–61. [CrossRef]
21. Lv, C.W.; He, J.; Zuo, L.; Vogt, R.D.; Zhu, L.; Zhou, B.; Mohr, C.W.; Guan, R.; Wang, W.Y.; Yan, D.H. Processes and their explanatory factors governing distribution of organic phosphorous pools in lake sediments. *Chemosphere* **2016**, *145*, 125–134. [CrossRef]
22. Murphy, J.; Riley, J.P. A modified single solution method for the determination of phosphate in natural waters. *Anal. Chim. Acta* **1962**, *27*, 31–36. [CrossRef]
23. Chen, Q.; Chen, J.A.; Wang, J.F.; Guo, J.Y.; Jin, Z.F.; Yu, P.; Ma, Z. In situ, high-resolution evidence of phosphorus release from sediments controlled by the reductive dissolution of iron-bound phosphorus in a deep reservoir, southwestern China. *Sci. Total Environ.* **2019**, *666*, 39–45. [CrossRef] [PubMed]
24. Ding, S.M.; Han, C.; Wang, Y.P.; Yao, L.; Wang, Y.; Xu, D.; Sun, Q.; Williams, P.N.; Zhang, C.S. In situ, high-resolution imaging of labile phosphorus in sediments of a large eutrophic lake. *Water Res.* **2015**, *74*, 100–109. [CrossRef] [PubMed]
25. Crusius, J.; Anderson, R.F. Core Compression and Surficial Sediment Loss of Lake Sediments of High Porosity Caused by Gravity Coring. *Limnol. Oceanogr.* **1991**, *36*, 1021–1031. [CrossRef]

26. Hupfer, M.; Gfichter, R.; Giovanoli, R. Transformation of phosphorus species in settling seston and during early sediment diagenesis. *Aquat. Sci.* **1995**, *57*, 305–324. [CrossRef]

27. Rita, J.C.D.O.; Gama-Rodrigues, A.C.; Gama-Rodrigues, E.F.; Zaia, F.C.; Nunes, D.A.D. Mineralization of organic phosphorus in soil size fractions under different vegetation covers in the north of Rio de Janeiro. *Content Uploaded Emanuela Gama-Rodrigues* **2013**, *37*, 1207–1215. [CrossRef]

28. Hupfer, M.; Lewandowski, J. Retention and early diagenetic transformation of phosphorus in Lake Arendsee (Germany)-consequences for management strategies. *Arch. Hydrobiol.* **2005**, *164*, 143–167. [CrossRef]

29. Xu, Y.; Han, F.E.; Li, D.P.; Zhou, J.; Huang, Y. Transformation of internal sedimentary phosphorus fractions by point injection of CaO_2. *Chem. Eng. J.* **2018**, *343*, 408–415. [CrossRef]

30. Stephen, D.; Moss, B.; Phillips, G. Do rooted macrophytes increase sediment phosphorus release? *Hydrobiologia* **1997**, *342*, 27–34. [CrossRef]

31. Søndergaard, M.; Jensen, J.P.; Jeppesen, E. Role of sediment and internal loading of phosphorus in shallow lakes. *Hydrobiologia* **2003**, *506–509*, 135–145. [CrossRef]

32. Wang, Y.; Ding, S.M.; Wang, D.; Sun, Q.; Lin, J.; Shi, L.; Chen, M.S.; Zhang, C.S. Static layer: A key to immobilization of phosphorus in sediments amended with lanthanum modified bentonite (Phoslock®). *Chem. Eng. J.* **2017**, *325*, 49–58. [CrossRef]

33. Christiansen, N.H.; Andersen, F.Ø.; Jensen, H.S. Phosphate uptake kinetics for four species of submerged freshwater macrophytes measured by a 33P phosphate radioisotope technique. *Aquat. Bot.* **2016**, *128*, 58–67. [CrossRef]

34. Xu, Q.S.; Fu, Y.Y.; Min, H.L.; Cai, S.J.; Sha, S.; Cheng, G.Y. Laboratory assessment of uptake and toxicity of lanthanum (La) in the leaves of Hydrocharis dubia (Bl.) Backer. *Environ. Sci. Pollut. Res.* **2012**, *19*, 3950–3958. [CrossRef]

35. Wang, X.; Shi, G.X.; Xu, Q.S.; Xu, B.J.; Zhao, J. Lanthanum- and cerium-induced oxidative stress in submerged Hydrilla verticillata plants. *Russ. J. Plant Physiol.* **2007**, *54*, 693–697. [CrossRef]

36. Herrmann, H.; Nolde, J.; Berger, S.; Heise, S. Aquatic ecotoxicity of lanthanum-A review and an attempt to derive water and sediment quality criteria. *Ecotoxicol. Environ. Saf.* **2016**, *124*, 213–238. [CrossRef] [PubMed]

37. Slomp, C.P.; Mort, H.P.; Jilbert, T.; Reed, D.C.; Gustafsson, B.G.; Wolthers, M. Coupled dynamics of iron and phosphorus in sediments of an oligotrophic coastal basin and the impact of anaerobic oxidation of methane. *PLoS ONE* **2013**, *8*, e62386. [CrossRef]

38. Mu, Z.; Wang, Y.C.; Wu, J.K.; Cheng, Y.; Lu, J.; Chen, C.C.; Zhao, F.X.; Li, Y.; Hu, M.M.; Bao, Y.F. The influence of cascade reservoir construction on sediment biogenic substance cycle in Lancang River from the perspective of phosphorus fractions. *Ecol. Eng.* **2020**, *158*, 106051. [CrossRef]

39. Kwak, D.H.; Jeon, Y.T.; Duck, H.Y. Phosphorus fractionation and release characteristics of sediment in the Saemangeum Reservoir for seasonal change. *Int. J. Sediment Res.* **2018**, *33*, 250–261. [CrossRef]

40. Dittrich, M.; Chesnyuk, A.; Gudimov, A.; McCulloch, J.; Quazi, S.; Young, J.; Winter, J.; Stainsby, E.; Arhonditsis, G. Phosphorus retention in a mesotrophic lake under transient loading conditions: Insights from a sediment phosphorus binding form study. *Water Res.* **2013**, *47*, 1433–1447. [CrossRef]

41. Zak, D.; Kleeberg, A.; Hupfer, M. Sulphate-mediated phosphorus mobilization in riverine sediments at increasing sulphate concentration, River Spree, NE Germany. *Biogeochemistry* **2006**, *80*, 109–119. [CrossRef]

42. Cui, Y.; Xiao, R.; Xie, Y.; Zhang, M.X. Phosphorus fraction and phosphate sorption-release characteristics of the wetland sediments in the Yellow River Delta. *Phys. Chem. Earth* **2018**, *103*, 19–27. [CrossRef]

43. Yang, J.X.; Tam, N.F.Y.; Ye, Z.H. Root porosity, radial oxygen loss and iron plaque on roots of wetland plants in relation to zinc tolerance and accumulation. *Plant. Soil* **2013**, *374*, 815–828. [CrossRef]

44. Canfield, D.E.; Thamdrup, B.; Hansen, J.W. The anaerobic degradation of organic matter in Danish coastal sediments: Iron reduction, manganese reduction, and sulfate reduction. *Geochim. Cosmochim. Acta* **1993**, *57*, 3867–3883. [CrossRef]

45. Tiessen, H.; Stewart, J.W.B.; Cole, C.V. Pathways of Phosphorus Transformations in Soils of Differing Pedogenesis. *Soil Sci. Soc. Am. J.* **1984**, *48*, 853–858. [CrossRef]

46. Rydin, E. Potentially mobile phosphorus in Lake Erken sediment. *Water Res.* **2000**, *34*, 2037–2042. [CrossRef]

47. Zhang, L.; Zhou, Q.; Liu, J.Y.; Chang, N.; Wan, L.H.; Chen, J.H. Phosphate adsorption on lanthanum hydroxide-doped activated carbon fiber. *Chem. Eng. J.* **2012**, *185–186*, 160–167. [CrossRef]

48. Zhang, L.; Liu, Y.H.; Wang, Y.L.; Li, X.H.; Wang, Y.Y. Investigation of phosphate removal mechanisms by a lanthanum hydroxide adsorbent using p-XRD, FTIR and XPS. *Appl. Surf. Sci.* **2021**, *557*, 149838. [CrossRef]

49. Pennafirme, S.; Pereira, D.C.; Pedrosa, L.G.M.; Machado, A.S.; Silva, G.O.A.; Keim, C.N.; Lima, I.; Lopes, R.T.; Paixão, I.C.N.P.; Crapez, M.A.C. Characterization of microbial mats and halophilic virus-like particles in a eutrophic hypersaline lagoon (Vermelha Lagoon, RJ, Brazil). *Reg. Stud. Mar. Sci.* **2019**, *31*, 100769. [CrossRef]

50. Rasuk, M.C.; Fernandez, A.B.; Kurth, D.; Contreras, M.; Novoa, F.; Poire, D.; Farias, M.E. Bacterial Diversity in Microbial Mats and Sediments from the Atacama Desert. *Microb. Ecol.* **2016**, *71*, 44–56. [CrossRef]